Experimental Observation and Statistics of Multipath from Terrain with Application to Overland Height Finding

Lisa M. Zurk

***Abstract*— Data is presented from an airborne experiment designed to evaluate electromagnetic pulse scattering from a variety of terrain types for the application of overland height finding. The one-way propagation data was collected at ultrahigh frequency (UHF) and very high frequency (VHF) frequencies using a 3-MHz pulsed CW signal with the radars mounted on two aircraft. A statistical analysis of the data shows that the probability of a detectable ground reflection and the strength of that reflection vary as a function of the terrain roughness. We introduce a broad-band synthesis technique in which Fourier theory is used to generate a time-domain response from a CW propagation model. Results from this technique agree well with the experimental observations, but the lack of detailed terrain information does not allow exact reproduction of the fine details.**

I. Introduction and Overview

THE subject of electromagnetic scattering from random rough surfaces has received considerable attention in recent years [1]. One area of interest is the interaction of electromagnetic energy with geophysical terrain. This field is an important one for the topics such as remote sensing [2], [3], telecommunications [4], [5] and evaluation of radar performance [6], [7]. In all of these areas, it is necessary to understand the complicated interaction of the electromagnetic wave with variable terrain and land surfaces and to ascertain the applicability of propagation models [8]. Much of the experimental data has been collected for low-angle backscatter from the ocean [9] and millimeter scattering from terrain [10], [11]. In this paper, we examine the nature of radiowave pulse scattering from various terrain types with the goal of evaluating the feasibility of overland height finding [12]–[14].

Many surveillance radars are not capable of using antenna beamforming techniques to determine target height. One method of providing this capability is to observe the time difference of arrival (TDOA) between the direct and reflected pulses. In a simple propagation scenario, the relationship between the observed TDOA and the target height is well understood and can be inverted. This is the scenario for propagation over water where TDOA height finding works reasonably well. However, when propagation occurs over irregular terrain the physics of the propagation are more complicated and it is uncertain whether or not a ground reflection will even be observed.

Manuscript received August 26, 1997; revised July 23, 1998.
The author is with MIT Lincoln Laboratory, Lexington, MA 02173 USA.
Publisher Item Identifier S 0018-926X(99)02206-1.

To evaluate the feasibility of overland height finding MIT Lincoln Laboratory engaged on an airborne data collection campaign in fall 1996, two aircraft were equipped with very high frequency (VHF) and ultrahigh frequency (UHF) antennas, which transmitted and received a 3-MHz pulsed CW signal. The purpose of the experiment was to observe the complex one-way propagated electric field as a function of terrain type. Large numbers of observations for each terrain type were obtained in order to provide enough data for statistical analysis of the results.

The propagation data was also compared to the results of several propagation models to determine the region of applicability of each model. Since the propagation models are single frequency models, a broad-band Fourier synthesis technique was utilized to rigorously generate time-domain results. This paper presents the results of this comparison.

The organization of this paper is as follows. The experimental investigation is described in Section II. Section III describes the propagation modeling and includes the Fourier techniques used to synthesize a time-domain response from a frequency-dependent propagation model. In Section IV, we present comparisons between the measured data and the synthesized data. The statistics of the reflected pulses analyzed as a function of the terrain type are presented in Section VII. We present our conclusions in the final section.

II. Propagation Experiment

To experimentally investigate the physics of multipath over variable terrain MIT Lincoln Laboratory engaged on a data collection campaign during September and October of 1996, over 2000 VHF and UHF data groups of 138 pulses each were collected during eight flights in New Mexico and northern Maine. The experiment used two airborne platforms to obtain data illustrating the effect of varying terrain type on electromagnetic propagation and bistatic clutter. The platforms were flown in two basic formations and the exact location of each aircraft was recorded with an on-board global positioning system (GPS). The first of the two flight formations was a parallel flight path with range distances on the order of 100 km. This formation was used for all the data presented in this paper. Bistatic clutter data was obtained at closer ranges with orthogonal and chase flights paths.

The two airplanes used in the experiment were a Cessna 421 and a Beechcraft 90 King Air. Both airplanes were equipped

TABLE I
RADAR PARAMETERS FOR MODE 1 DATA

Tx PRF (Hz)	TX pulse width (μs)	Rx PRF (Hz)	f_s (MHz)	# RANGE GATES	# PRIs	TOTAL TIME (CPI) (s)
2500	0.333	2	4.0	1800	138	69

with VHF and UHF H-pol and V-pol antennas that were operated at 141 and 431 MHz, respectively. The Cessna had a belly-mounted VHF whip antenna for V-pol radiation and a portside circular patch antenna for UHF radiation (both polarizations). It also utilized a modified glide-slope antenna on the starboard that resembles a "towel bar" for the VHF H-pol radiation. The King Air had a belly-mounted monopole for V-pol radiation and a tail mounted dipole for H-pol radiation; the antenna elements were switched to change from VHF to UHF.

The Cessna transmitted a pulsed CW signal that was received on the King Air and recorded. Synchronization between the transmit and receive systems was attained by choosing the receive pulse-repetition interval (PRI) to be an integral multiple of the transmit PRI and by choosing a data collection window that was at least as large as the transmit PRI. These two restrictions assured that: 1) at least one pulse would be captured every PRI and 2) the pulse would appear in the same range gate across a coherent processing interval (CPI) if there was zero doppler and if the oscillators were perfectly matched.

Although three different modes of operation were used to record data, only the data collected in Mode 1 will be presented in this paper. Mode 1 is called "slow" mode since the data was collected at a 2-Hz pulse-repetition frequency (PRF). The movement of the platforms during the 0.5 s intervals between two consecutive pulses allowed a large number of statistically independent samples of a particular terrain type to be collected. Table I gives the radar parameters for the experiment.

III. PROPAGATION MODELING AND PULSE SYNTHESIS

In this paper, we will consider two propagation models: spherical earth and the spherical-earth-knife-edge (SEKE) model developed at MIT Lincoln Laboratory [15]. These models will be used to generate frequency dependent, complex electric fields quantities that can be used to synthesize pulses. The goal is to use the GPS information from the experiment to generate inputs to drive the propagation models. If the inputs are known perfectly and the models are sufficiently rigorous, the synthesized results should match the observed data. The pulse-synthesis procedure is shown diagrammatically in Fig. 1.

It is worthwhile to note that because it is our intent to compare the output of these models with that obtained experimentally, we will discuss geometries with a one-way propagation path. However, the results can easily be extended to a two-way propagation scenario by exploiting electromagnetic reciprocity.

A. Spherical Earth Model

The spherical earth model is a ray model that geometrically computes the path-length difference between the direct and reflected propagation paths, as shown in Fig. 2, with dashed lines indicating ray paths from the transmitter to the receiver. The refractive nature of the atmosphere is taken into account using an effective earth radius in the computations (e.g., "4/3 earth approximation"). Under this model the path-length difference between the direct and ground reflected paths Δr can be written as

$$\Delta r = 2z_1' z_2'/R \tag{1}$$

where z_1' and z_2' are the transmitter and receiver heights, respectively, with the primes indicating an earth flattening transformation that maps the spherical earth into an equivalent planar geometry [16].

In a pulsed radar system, multiple propagation paths can result in pulses arriving at the receiver staggered in time. The time difference between receipt of the pulse following the direct path and that reflected off of the ground is called the TDOA and is given by $\Delta t = \Delta r/c$. The TDOA will only be observed if the radar resolution δr is less than or equal to the path-length difference; otherwise the pulses will overlap in time and the field at the receiver will be a coherent addition of the two rays.

In surveillance radars, the observed TDOA can be inverted using the spherical earth model to yield the target height z_2. Height finding in this manner is useful for propagation over the ocean where geometrical optics is valid and the surface is fairly

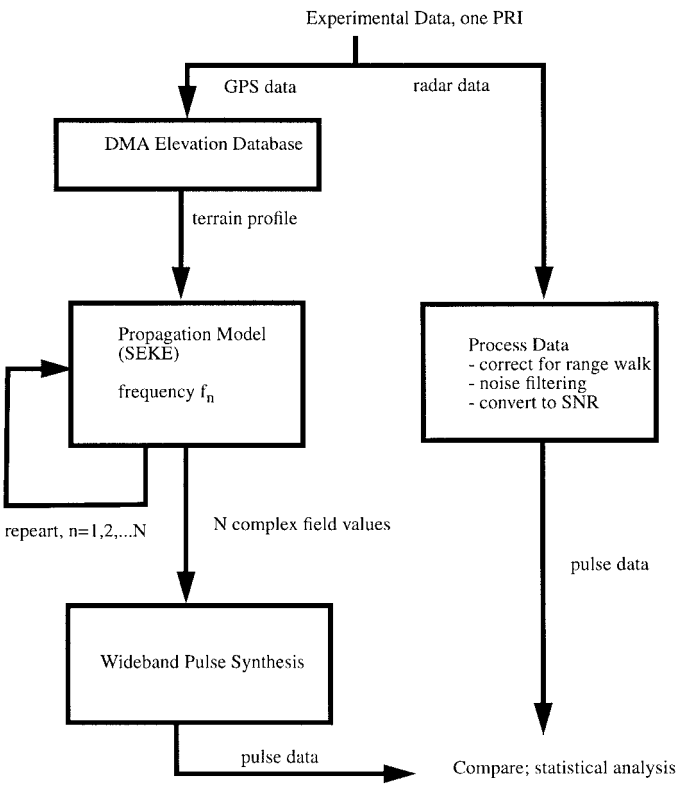

Fig. 1. Diagram representing the pulse synthesis procedure for a single PRI; the process is repeated for all 138 PRIS in a data group. This diagram shows that the wide-band pulse-synthesis technique (2) requires the propagation model to be run N times to generate a frequency-dependent response (present paper uses $N = 256$). If the model is computationally expensive this could prove unfeasible. The ray sum approach (not shown) runs the model once to generate the amplitude and path length each of the Ns rays [see (4)].

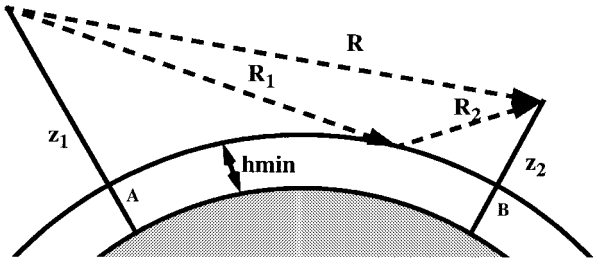

Fig. 2. Geometry for a spherical earth model showing direct and ground bounce paths for one-way propagation. The receiver and transmitter are located at MSL altitudes $z1$ and $z2$, respectively, and there is a mean elevation of $hmin$ in the area of interest. The direct path distance is R and the path length difference is $Dr = (R1 + R2) - R$. The range distance r is the arc length between A and B.

flat, good reflector. However, when the propagation occurs over terrain the situation becomes much more complicated. Terrain features can be highly variable and introduce scattering and diffraction phenomenon that effect the electromagnetic wave propagation. Investigating how the presence of these features effects the propagation physics and how the observed TDOA differs from that predicted by a spherical earth model was one of the goals of this effort.

B. Spherical Earth Knife Edge (SEKE)

For propagation over irregular terrain, the electromagnetic field can include contributions from multiple specular points, knife-edge diffraction, and spherical-earth diffraction. The spherical earth knife edge (SEKE) model developed at MIT Lincoln Laboratory [15] combines these effects to estimate the multipath factor F^2. To produce a time-domain signal we modified SEKE to obtain the complex electric field quantities over a frequency band of interest and synthesized a pulse from this field as described in the following subsection.

For the propagation geometries in the airborne experiment the geometric optics portion of SEKE was activated. In this calculation, SEKE moves along the terrain profile identifying unmasked specular points on the terrain where the local slope satisfies Snell's law and supports a reflected ray directed toward the receiver. The field at the receiver is the coherent sum of all the specular rays, which can add destructively or constructively.

SEKE requires as input a uniformly spaced profile representing the terrain elevation between the transmitter and receiver. The airborne data collection had range distances on the order of 100-130 km in length with the exact position of each plane recorded by an on-board GPS. The terrain elevation profile for each given pulse was constructed by combining the time stamp in the data with the GPS data to determine aircraft position and then interpolating defense mapping agency (DMA) data to generate a profile with uniform horizontal spacing of 96 m.

C. Pulse Synthesis

The time-dependent electric field for a pulsed radar $E_t(t_n)$ can be represented as an inverse Fourier transform of the frequency dependent complex electric field $E(f)$

$$E_t(t) = \sum_{j=-N/2}^{(N/2)-1} E(f_j) W(f_j) e^{i2\pi f_j t} \tag{2}$$

where $f_j = f_0 + j\Delta f$, f_0 is the center frequency and $j = 0, 1, \cdots, N-1$. The function $W(f_j)$ is a windowing function that represents the frequency response of the receiver and serves to bandlimit the response. For a given $W(f_j)$, the transform in (2) is an exact equation for the time-domain response provided that the complex electric field is known across the frequency band of interest. Therefore, one approach to determining E_t is to calculate the propagated electric field for a series of tones f_j and then to compute $E_t(t)$ via the transform in (2). This approach will be termed the wide-band synthesis approach.

Under a geometrical optics formulation the complex electric field can be written as a sum of the field due to the direct ray and the field from the N_s reflected rays arising from the multiple specular points on the terrain

$$E(f_j) = \exp\left(-i2\pi f_j \frac{R}{c}\right) + \sum_{\upsilon=1}^{N_S} A_\nu(f_j) \exp\left(-i2\pi f_j \frac{R + \Delta r_\upsilon(f_j)}{c}\right) \tag{3}$$

where c is the speed of light in free-space, R is the direct path length, and Δr_υ and A_υ are the frequency dependent path-length difference and amplitude of the ray originating from the υth reflection point, respectively. If the propagation occurs over a smooth spherical earth, $N_S = 1$ and (3) reduces to the well-known multipath expression whose magnitude squared accounts for the propagation loss.

An important property of Fourier signals is that complex modulation in the frequency domain corresponds to a shift in the time domain. Equation (3) can be simplified considerably by assuming the A_υ is constant over the bandwidth of the system. In this case, substitution of (3) into (2) and application of the linearity of the Fourier transform yields a time-domain response that is the superposition of shifted pulses

$$E_t(t) = W_t(t - t_d) + \sum_{\upsilon=1}^{N_S} A_\nu W_t(t - t_d - \Delta t_\upsilon) \tag{4}$$

where the first term is the direct path pulse arriving at $t = t_d = R/c$ and W_t is the inverse Fourier transform of $W(f)$. The terms in the summation arrive later in time by Δt_υ and may or may not be separated from the direct pulse depending on the pulse width of W_t. It should be noted that (4) can only be used if a ray model is appropriate and if all the paths lengths are explicitly known. In addition, the summation must be done coherently as the complex amplitudes A_υ will generate constructive and destructive interference. Pulse synthesis using (4) will be called the ray-sum synthesis approach.

TABLE II
FLIGHT PARAMETERS FOR FIGURES

Figure	Freq. (MHz)	Pol.	Cessna Alt. (kft) MSL	King Air Alt. (kft) MSL	Rng. (km)	flight date (1996)	Location
Fig. 3	431	v	15.0	20.0	100	9/21	WSMR, NM
Fig. 4	431	h	20.0	13.0	130	9/21	WSMR, NM
Fig. 5	141	h	20.0	20.0	130	9/22	WSMR, NM
Fig. 6	141	h	20.0	15.0	130	9/22	WSMR, NM
Fig. 8	141	h	17.5	17.5	100	9/19	WSMR, NM
Fig. 12	141	h	9.5	17.5	100	10/7	Millinocket, ME

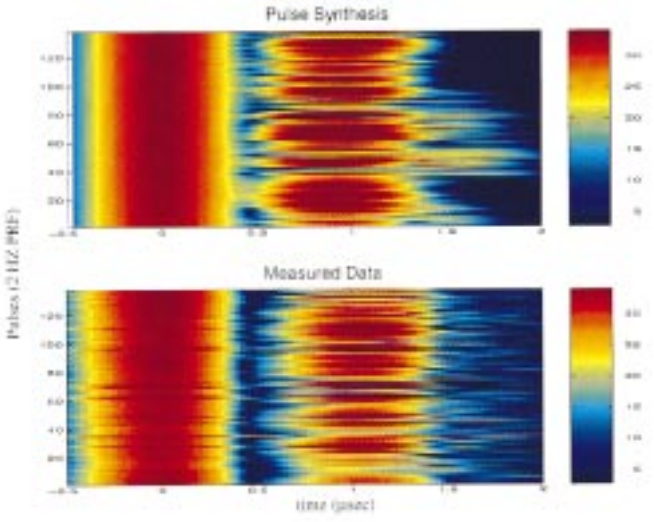

Fig. 3. SNR levels in decibels from UHF V-pol data obtained in WSMR. The strong presence of a multipath return is captured by the simulation.

IV. COMPARISON OF PROPAGATION DATA WITH SYNTHESIZED PULSES

In this section, we present comparisons between measured and simulated data. The comparisons are presented in the form of color plots where the color levels correspond to signal-to-noise ratio (SNR) and the direct pulse is shown arriving at time $t = 0$. The dashed line represents the TDOA predicted using a spherical earth formula. Table II gives the flight parameters for each of the plots.

Figs. 3 and 4 show results from UHF flights in White Sands missile range (WSMR) on September 21st. The agreement between the actual and simulated data is quite good. For example, Fig. 3 is from a V-pol flight where the specular point lay on fairly smooth flat desert terrain. The data shows that terrain supported a strong multipath for the majority of the pulses. This strong response and the time delay relative to the direct pulse is captured by the simulated data as well. It is important to note that the simulations cannot reproduce the fine details seen the radar data due to the coarseness of the terrain characterization (i.e., the DMA data). This point will be discussed in more detail further in the manuscript.

In Fig. 4, the Fresnel zone had shifted onto the foothills of the San Mateos mountain range where the terrain is no longer flat. For a substantial portion of the CPI the nature of the

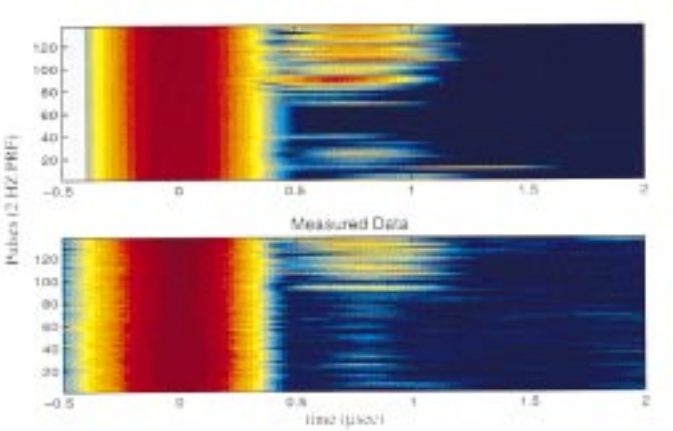

Fig. 4. SNR levels in decibels from UHF H-pol data obtained in WSMR. Because of the tilt of the terrain, the pulses at the beginning of the data group do not generate reflections while the later pulses do produce a multipath return. This behavior is seen in both the measured data and the synthesized pulses (SNR levels are the same as Fig. 3).

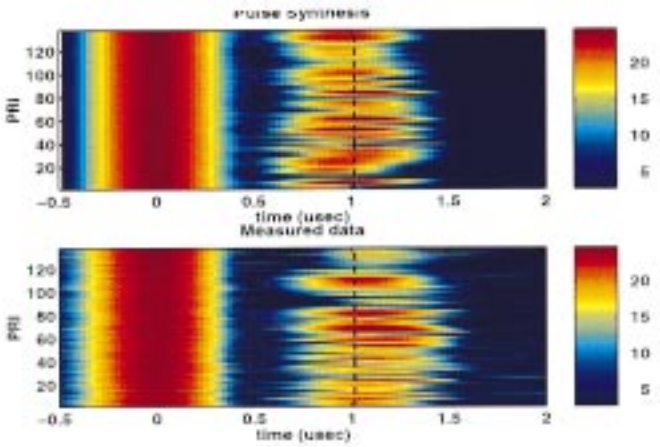

Fig. 5. SNR levels in decibels from VHF H-pol data obtained in WSMR. The Fresnel zone lay across the smooth desert floor. The spherical earth formula predicts a TDOA of 1.02 ms (shown as a dashed line).

terrain is such that it did not support a ground reflection. For both the measured and simulated data this is clearly seen in the first part of the coherent processing interval (CPI) where a multipath return is not present. It is reasonable to expect that the increasing roughness of the terrain at the specular point diminishes the intensity of the multipath return where it is present. This is seen in the low specular return in the data relative to that seen in Fig. 3. The simulated data predicts a slightly higher ground reflection because the coarseness of the DMA profiles does not include the small scale roughness that will serve to diffuse the scattering.

The plots in Figs. 5 and 6 are VHF H-pol data from WSMR collected on September 22nd. These flights were structured so that as the King Air descended, the Fresnel zone moved from the desert floor (Fig. 5) into mountainous terrain (Fig. 6). As the terrain becomes successively rougher, more energy can be observed arriving at the receiver with a TDOA that is longer than that estimated by the spherical earth formula. In addition, the TDOA is much more variable and spans a wider range

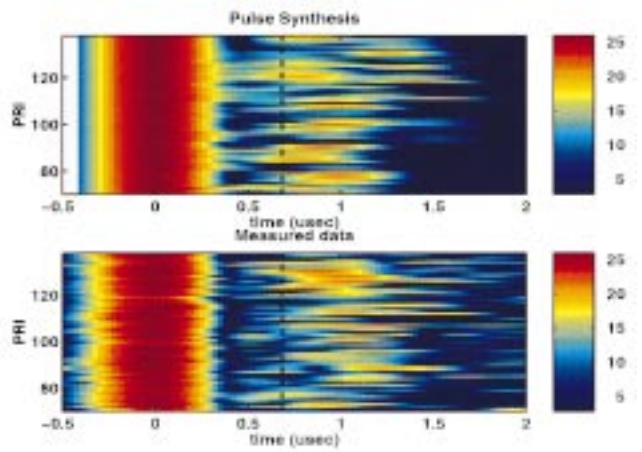

Fig. 6. SNR levels in decibels from VHF H-pol data obtained in WSMR. The Fresnel zone lay across rough mountainous terrain that contains many disparate random scatterers. This randomness serves to destroy the coherent nature of the multipath return. The spherical earth formula predicts a TDOA of 0.68 ms (shown as a dashed line).

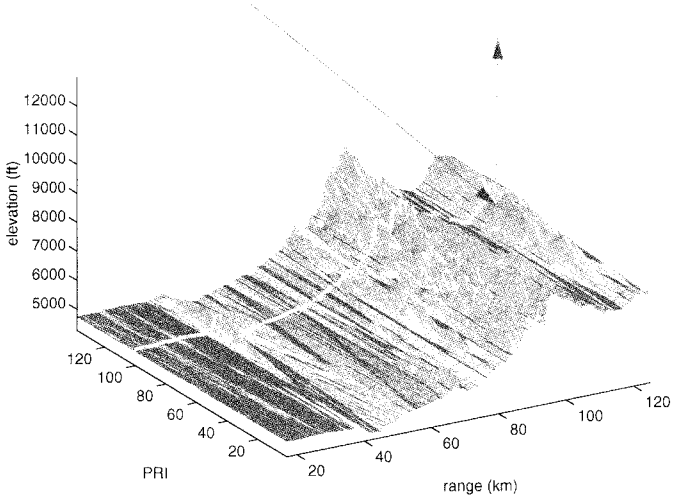

Fig. 7. Terrain for the data shown in Fig. 6. The red line shows the terrain profile for the 100th pulse of the data group and the yellow asteriks show the 15 specular points identified by SEKE. The ray path from the transmitter to the receiver for the last specular point is indicated by arrows.

of values. A surface plot produced from the DMA data for the mountainous terrain is shown in Fig. 7. As an example, consider the elevation profile for the 100th pulse that is drawn as a red line. The reflection point according to a spherical earth model would be 80 km from the transmitter, but the irregular terrain at this location prevents energy from being reflected and seen at the receiver. However, SEKE identifies 15 additional specular points along the terrain. The ray reflecting from the furthest of these points is indicated by arrows in the figure. Note that since the path length traveled by these rays is longer than that for a ray reflecting at the 80-km point, the observed TDOA is longer than the spherical earth predication, as was seen in Fig. 6.

The terrain dependence discussed above was observed for both the VHF and UHF data. In fact, at these small grazing angles the radar data showed little difference between the two frequencies for any of the terrain types, except for differences in power levels that were attributable to the separate transmitters and antennas.

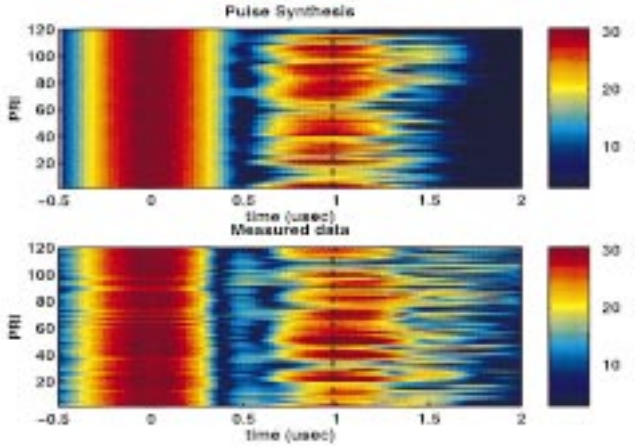

Fig. 8. SNR levels in decibels from VHF H-pol data obtained in WSMR. The Fresnel zone lay across the gently rolling desert floor.

V. Comparison of Individual Synthesized Pulses with Measured Data

In this section, we compare more closely the synthesized pulses with the measured data. We show that although the synthesized data accurately reproduces the macroscopic features of the multipath, it is unable to generate the fine details. This limitation is most likely due to the insufficient characterization of the terrain and atmosphere. However, since we are interested in the average or statistical nature of the reflected pulses, it may not be necessary to match the fine details. In the following section, we show that the statistics of the measured and simulated data are in agreement.

The plots in Fig. 8 are VHF H-pol data from WSMR where the underlying terrain was smoothly rolling desert floor. For the majority of the pulses a strong multipath response is observed and the character and TDOA of the multipath is well reproduced by simulation. However, some of the pulses produce a diminished ground reflection. Unlike the example in Fig. 6 where the terrain was quite rough, this is not due to pronounced irregularities in the underlying terrain, but rather to the destructive addition of multiple reflections. This results in a coherent cancellation exactly analogous to that which occurs in multipath nulling. To illustrate this point, we examine more closely the propagation physics for the first and 110th pulse or PRI of the data group shown in the first plot of Fig. 8.

The elevation profiles for these two pulses are shown in Fig. 9, with the aircraft denoted as circles. The asterisks in the figure signify the location of the 15 specular points identified by a SEKE simulation at the center VHF frequency of 141 MHz. Energy from the transmitter will reflect off the terrain at each of the specular points and some portion will be redirected toward the receiving antenna. This is indicated by the arrows in the figure for a specular point a distance of 77 km from the transmitter. The time-domain response for these pulses was calculated by both wide-band synthesis and ray-sum synthesis and is shown in Fig. 10 along with the measured data and

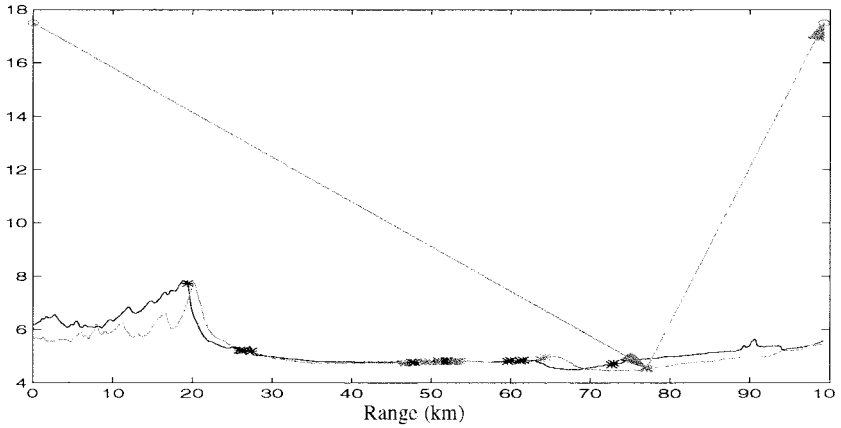

Fig. 9. Elevation profile for the first and 110th pulses for the data group shown in Fig. 8. The 15 specular points identified by SEKE are indicated as asterisks. The arrows represent a ray reflecting off of the terrain at a range distance of 77 km from the transmitter and resulting in a pulse with a TDOA of 1.44 ms. Note that for the pulse to be discernible that receive antenna must have sufficient elevation bandwidth.

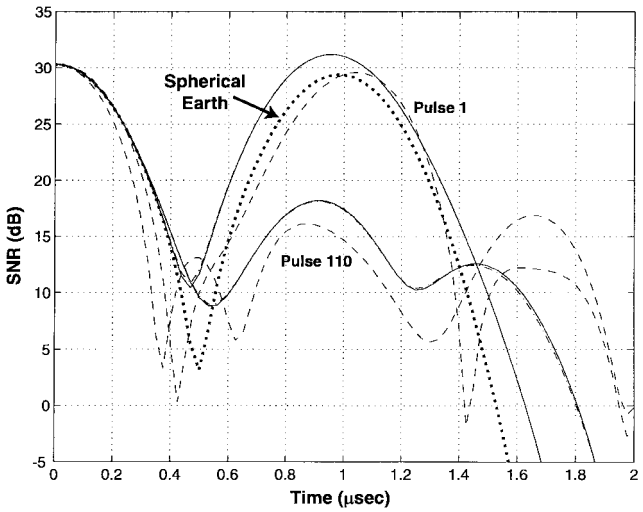

Fig. 10. The time-domain response of the first and 110th pulses in the data group shown in Fig. 8. The simulations follow the data fairly well, with the wide-band synthesis and the ray-sum synthesis overlaying each other. Note the difference in the level of the multipath return for the two pulses due to the destructive and constructive nature of the multiple speculars. The energy seen in the measured data arriving at 1.6 ms after the direct pulse is most likely due to the presence of out-of-plane scatterers not considered in the SEKE model. The line legend is wide-band synthesis (solid), ray-sum synthesis (dash-dot), measured data (dashed), and spherical earth model (dotted).

a pulse synthesized using the results of a spherical earth prediction. The figure shows ray-sum synthesis and wide-band synthesis give nearly identical results for this banwidth.

The synthesized data predicts that the reflection for the first pulse will have a signal level that is slightly higher than the direct pulse due to the constructive addition of the specular reflections whereas the reflection from the 110th pulse is significantly attenuated due to destructive addition. The signal predicted under the pulse synthesis agrees fairly well with the measured data but the exact shape of the pulse is not reproduced accurately. For the 110th pulse, there is a third arrival 1.44 μs after the direct pulse. This energy is from an additional specular point on the great circle path and corresponds to the ray indicated by arrows in Fig. 9. One feature seen in the data but not produced in the simulation is additional pulses arriving approximately 1.75 μs after the direct pulse. It is probable that this contribution is due to out-of-plane scatterers that are not taken into account in the modified SEKE model.

A second source of error in producing agreement between simulated and actual pulses is the limitations of the terrain data that was used to drive the propagation model. For example, consider the data obtained in northern Maine over a wooded hilly terrain. The top plot of Fig. 13 shows the elevation profile for the great circle path as obtained from two different agencies: Defense Mapping Agency (DMA) and U.S. Geological Survey (USGS). The differences between the two profiles are hardly noticeable on the scale of the plot but have a pronounced effect on the CW multipath lobes. The multipath factor is shown in the middle plot and has been computed using SEKE with the two different elevation profiles as input. As can be seen from the plot, SEKE predicts a 5-dB enhancement on a 5334-m target when the DMA data is used as input, but for the same height target it predicts a deep multipath null when

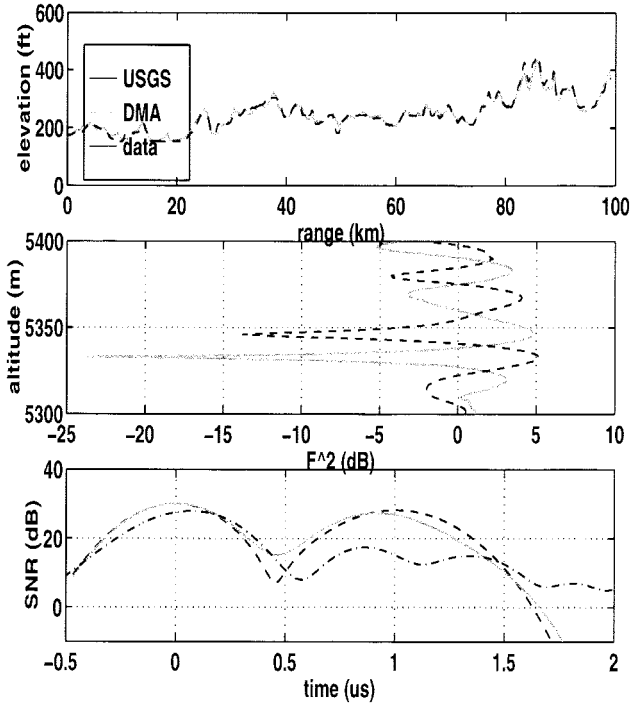

Fig. 11. VHF H-pol data from Maine. The top plot shows the elevation profile for the great circle path as given by the DMA data (dashed) and the USGS data (solid) for the first pulse in the data group. The middle plot shows the propagation factor F2 as a function of receiver height as computed by SEKE for the two profiles at 141 MHz. The last plot shows the result of a wide-band pulse synthesis plotted with the observed data (dash-dot). The results for the entire data group are shown in Fig. 12.

the USGS data is used. This result is not overly surprising since determining the exact location of the multipath lobes requires wavelength scale accuracy of the terrain profile. This sensitivity is offset to some degree when a broad-band system is employed. The final plots in the figure shows the predicted pulses for the two terrain profiles and the results are quite similar. The bandwidth of the system separates the direct and multipath response and the sensitivity to the coherent addition of the two is removed.

Also seen in the last plot is that the simulation fails to exactly duplicate the observed data. The TDOA is similar between the two but the details of the pulse shape are not accurately reproduced in the simulation. One possible explanation for the mismatch is that the 96-m resolution of the input data is too coarse. The wavelength at VHF is 2 m, thus, one would expect that the wave will respond to terrain features much smaller than the DMA information provides. Another possibility is that the error is due to a deficiency in the propagation model that is used to generate the pulses. Terrain is typically inhomogeneous and varying with range but SEKE allows only a single reflection coefficient to characterize the ground. It might be possible to use a more sophisticated model (such as a parabolic wave equation) to represent the presence of vegetation or other land cover with an effective permittivity (see Fig. 11).

Fig. 12 shows the observed and simulated pulses for the entire data group. As in the WSMR data, there is considerable variability in the observed data and in the simulation. We have

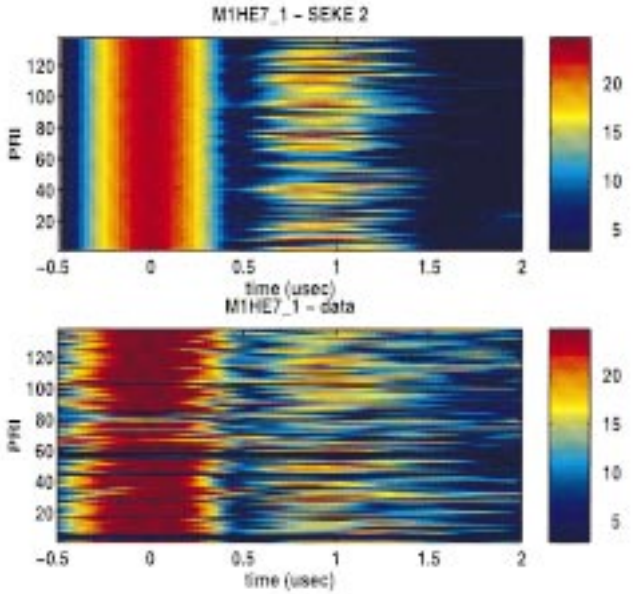

Fig. 12. SNR levels in decibels from VHF H-pol data obtained in northern Maine. The top plot is pulses simulated using SEKE with a wide-band synthesis. The bottom plot is the measured data which is considerably noisier than that obtained in New Mexico, but the presence of a multipath is still visible.

found that the general properties of the multipath response are captured by the simulated pulses but exact agreement on a pulse-to-pulse basis is not always possible.

VI. Discussion of Synthesis Techniques and Pulse Dispersion

In this section, we discuss the wide-band and the ray-sum synthesis methods and show that, as expected, they give numerically identical results for a reasonably narrow bandwidth. It is important to remember, however, that the ray-sum technique can only be employed when a geometric optics model is justified and when the amplitude, phase, and path length of every ray is explicitly known. The ray-sum synthesis method then simply consists of coherently summing of each of these rays weighted by the time-domain pulse shape. The wide-band synthesis technique can be applied regardless of the propagation physics provided that the magnitude and phase of the electric field at the receiver is known across the desired frequency band. Once this has been determined, the time-domain response is given by the inverse Fourier transform for the desired pulse shape. This effect will become more important as the bandwidth of the system is increased.

Fig. 13 shows the magnitude of the reflected electric field seen at the receiver over a 40-MHz band calculated by the wide-band and ray-sum methods. (It is instructive to note that a terrain generating only a single reflection would appear as a straight line with a magnitude given by the reflection coefficient of the ground.) The two techniques give nearly identical results at the center of the band, but begin to diverge at other frequencies. This is due to the assumption that the amplitude of the ray is constant over frequency and can be approximated by its value at the operating frequency. For very wide bandwidths, this assumption might not hold.

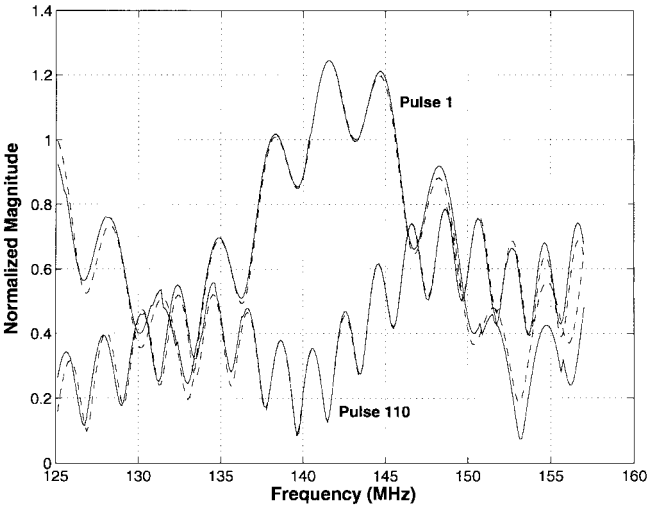

Fig. 13. The amplitude of the reflected electric field for the data group shown in Fig. 8. The top curve is for the first pulse and the bottom curve is for the 110th pulse; wide-band pulse synthesis is shown as a solid line and ray-sum synthesis as a dashed line. If there was a single specular reflection, the amplitude would be constant over the bandwidth with a value of the Fresnel reflection coefficient. The high- and low-frequency modulation of the reflected field is due to the destructive and constructive coherent addition of the multiple speculars. Note that the signal level at the center frequency (141 MHz) differs significantly for the two pulses, which is also observed in the time-domain behavior (Fig. 10).

The modulated field shown in Fig. 13 indicates the presence of multiple speculars and represents a dispersive environment. The increased field strength for the first pulse at 141 MHz is what produces the increased power in the multipath return in Fig. 10. Likewise, the decreased strength for the 110th pulse is what serves to degrade the multipath response. The frequency dependence will also serve to distort the time-domain pulse shape.

VII. Statistics of Measured and Simulated Data

In this section, we present plots showing the statistics of the measured and simulated data as a function of terrain type. The quantities of interest are: 1) the probability that a ground reflected pulse will be observed; 2) the strength of the reflected pulse; and 3) the TDOA relative to that predicted by spherical earth. It is important to note that the reflection strengths are given in units relative to the direct pulse. For specular reflections, this removes any antenna pattern dependency.

The presence of a ground reflected pulse was determined by a correlation analysis. A Gaussian pulse representing the transmitted pulse was shifted by a time delay of t_s and correlated with the time-domain response in each PRI of the measured and simulated data. A pulse at some delay t_s was considered to be present if it was at least 3 dB above the noise floor and had a SNR that was no lower than 13 dB below the direct pulse. If multiple ground reflections were detected in any one PRI, only the characteristics of the earliest arrival were considered in the statistical analysis. Results of this analysis are shown in Fig. 14 and Fig. 15 for the measured and simulated data, respectively. The terrain in this case produced the results in Fig. 8 and was smoothly rolling desert floor. It produced reflections with time delays close to that predicted by spherical earth and with little variance. For this

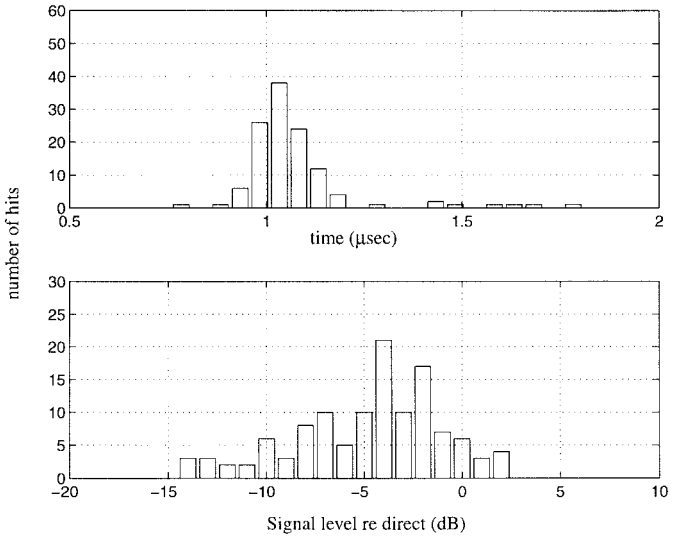

Fig. 14. Histograms produced from the measured data shown in the data group in the bottom of Fig. 8 (VHF H-pol from desert terrain in WSMR). The top plot shows the distribution of the observed time delays and the bottom plot shows the strength of the pulses relative to the direct. A total of 120 of the 138 pulses had identifiable ground reflections with a mean time delay of 1.05 ms (spherical earth predicts a 0.98-ms delay) and a mean signal level of -4.11 dB are the direct.

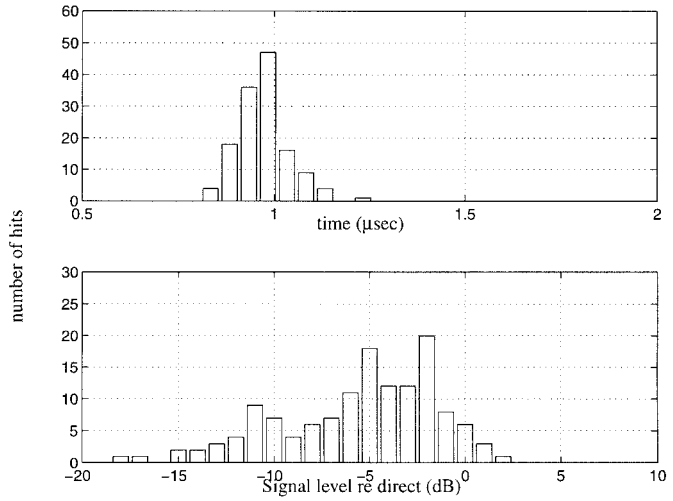

Fig. 15. Histograms produced from the simulated data shown in the data group in the top of Fig. 8 (VHF H-pol data from desert terrain in WSMR). The top plot shows the distribution of the observed time delays and the bottom plot shows the strength of the pulses relative to the direct. A total of 137 of the 138 pulses had identifiable ground reflections with a mean time delay of 0.l97 ms (spherical earth predicts a 0.98-ms delay) and a mean signal level of -4.97 dB are the direct.

terrain, a reflection was observed a significant proportion of the time with a fairly high signal level indicating the flat terrain was strongly reflective. This strong return is due to both the relatively high-reflection coefficient for low-grazing angles as well as the fact that the surface was flat and, thus, most of the energy was scattered specularly.

The histograms for the more irregular terrain (results shown in Fig. 6) are presented in Fig. 16 and Fig. 17. It can be seen from the figures that the variability of the terrain produces a much wider distribution of observed time delays and a much reduced signal strength. Both the simulated and the measured

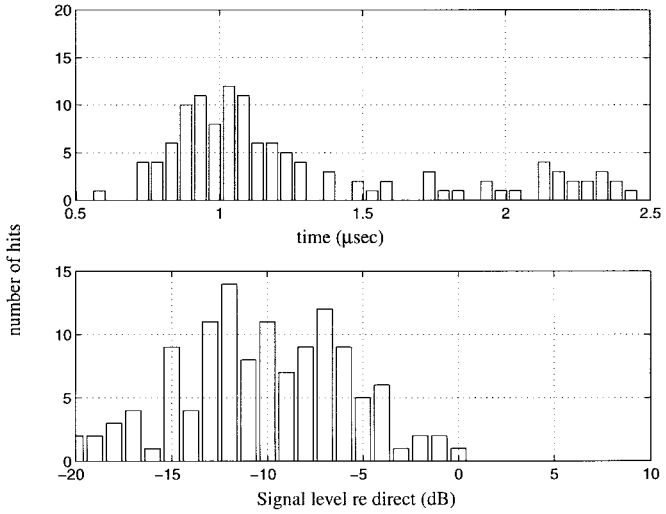

Fig. 16. Histograms produced from the measured data shown in the data group in the bottom of Fig. 6 (VHF H-pol data from mountainous terrain in WSMR). The top plot shows the distribution of the observed time delays and the bottom plot shows the strength of the pulses relative to the direct. A total of 123 of the 138 pulses had identifiable ground reflections with a mean time delay of 1.07 ms (spherical earth predicts a 0.68-ms delay) and a mean signal level of −10.11 dB are the direct.

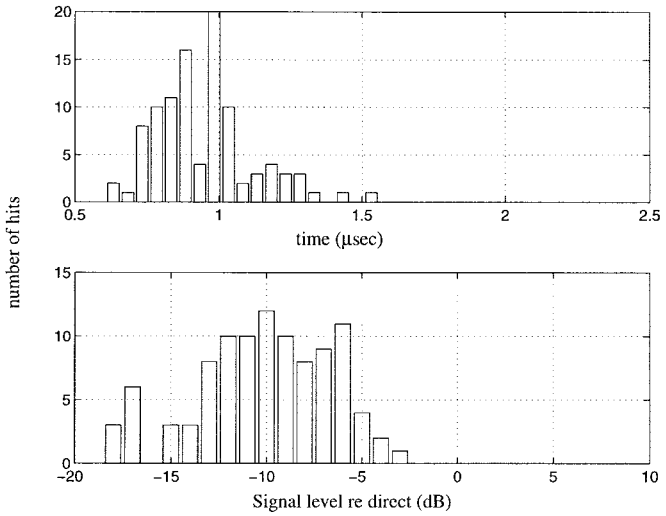

Fig. 17. Histograms produced from the simulated data shown in the data group in the top of Fig. 6 (VHF H-pol data from mountainous terrain in WSMR). The top plot shows the distribution of the observed time delays and the bottom plot shows the strength of the pulses relative to the direct. A total of 100 of the 138 pulses had identifiable ground reflections with a mean time delay of 0.93 ms (spherical earth predicts a 0.68-ms delay) and a mean signal level of −9.85 dB are the direct.

data show this trend in the statistics. However, the measured data shows a long tail in its time-delay distribution indicating the arrival of pulses with significant path-length differences. The presence of this tail could be due to strong out-of-plane scatterers such as the surrounding mountains that are not taken into account by an in-plane model such as SEKE.

The correlation analysis was repeated for all the Mode 1 data groups obtained in the propagation experiment. In Fig. 18, the plots shows (from top to bottom) the percent observed reflections, SNR of the reflection relative to the direct pulse, and the TDOA relative to a spherical earth prediction. All

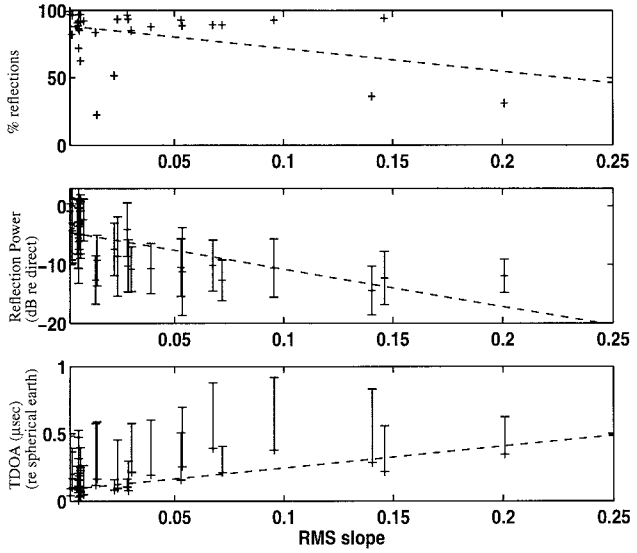

Fig. 18. Results of the correlation analysis for all mode 1 data groups. The plots are (from top to bottom): the percent of PRI's in which a detectable ground reflection is seen, the power of the reflection relative to the direct pulse, and the TDOA observed relative to that expected from a spherical earth prediction. All the quantities are plotted as a function of the rms slope along the great circle path from transmitter to receiver with the linear fit to the data shown as a dashed line. The bottom two plots have error bars at 1 σ level with the TDOA error being one sided as discussed in Section V. Each data point is the mean of the 138 PRI's in a data group.

quantities are plotted as a function of the root-mean-square (rms) roughness of the terrain from the DMA data within the first Fresnel zone and along the great circle path between the transmitter and the receiver. Each data point on the plots represents the average of the 138 pulses in a data group (e.g., the distribution shown in Fig. 14 had a mean TDOA of 1.05 μs). The plots contain the data from both the UHF and VHF flights at horizontal (HH) and vertical (VV) polarizations.

Several features in the plots can be observed. The top two plots show that the number of observed reflections and the strength of these reflections decrease as the terrain roughness increases, respectively. This is a result of the increasing rough terrain surface destroying the coherent specular reflection. In terms of a geometrical optics model, this decrease in amplitude of the reflected ray is due to the increase in the diffuse scattering coefficient. The existence of a relationship between surface roughness and ρ_d is well known (see, for example, [17]). One important point to note is that the surface elevation given by DMA data has a 96-m horizontal resolution. Thus, the rms roughness plotted in Fig. 18 is a *large* scale roughness—no information about the wavelength scale roughness is available.

The bottom plot shows the difference between the observed TDOA and that predicted by a spherical earth formula (1). As the terrain grows rougher, the spherical earth model is no longer applicable and its predictions for the TDOA become increasingly erroneous. For the application of overland height finding this indicates that although a TDOA may be observed over rough terrain, a substantial error is introduced if the target is determined using a spherical earth formula. This can also be seen in the plot in Fig. 19, which shows the results of target height estimation for each of the radar data sets versus the rms terrain roughness. The mean target height was calculated

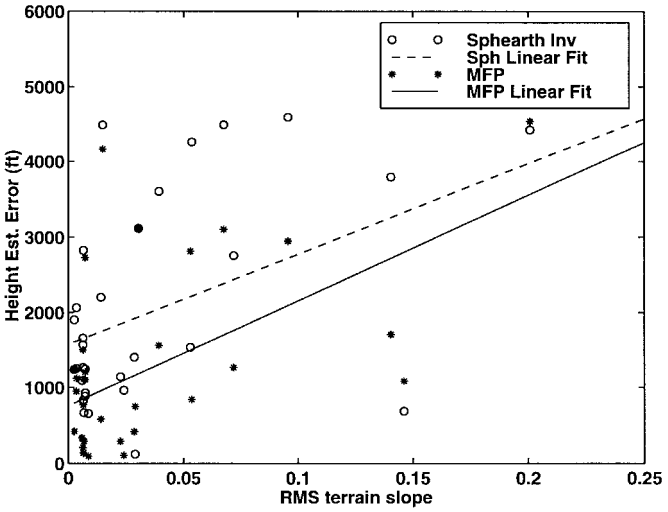

Fig. 19. Plot showing the absolute error between the mean height estimate for all data groups (both VHF and UHF) and the actual target height. The open circles are produced from the radar data by measuring the TDOA and applying the spherical earth formula in (1); the dashed line shows a linear fit. The asterisks are produced by applying a MFP algorithm with replica vectors generated from geometrical optics. Both techniques give more error for rougher terrain where the forward models are less likely to be accurate.

by two different methods. In the more simple method, the height estimation was achieved by measuring a time delay $\Delta t = \Delta r/c$ and inverting the spherical earth formula in (1) to determine the height z_1. As expected, the plot shows that the error increases as the terrain roughness increases and the spherical earth formula is no longer applicable.

An alternative method of determining target height is to employ an inversion scheme such as matched-field processing (MFP) [18]. The rationale of MFP is to use a sophisticated forward propagation model to propagate energy from a source at a hypothetical location to the receiver. This process is repeated for sources at all possible locations and then the resulting "replica" fields are compared or "matched" to those actually observed at the receiver to determine the most likely source location. The power of the MFP algorithm is that instead of ignoring the complicated environment, it exploits our knowledge of the physics of the propagation and it brings it to bear on the localization problem. The MFP algorithm originated in the acoustics community, but is recently receiving attention for application to tropospheric propagation [19], [20], [14]. To produce the results in Fig. 19, we used SEKE with DMA data as our forward model to generate pulse signatures for 100 target heights and then used MFP to determine the optimum. As seen in the plot, the performance is superior to the spherical earth inverstion, but it requires substantially more processing. Further details of the MFP processing can be found in [14].

VIII. Conclusions

This paper presents data from a recent airborne propagation experiment and compares these results with pulses synthesized using a modified SEKE model and Fourier techniques. In both the measured data and the simulated pulses, a detectable ground reflection is seen over a variety of terrain types for both VHF and UHF frequencies. The nature of this response depends on the terrain type and tends to decrease in strength and frequency of occurrence as the terrain grows rougher. More variable terrain also results in a TDOA that differs significantly from that predicted by a spherical earth formula. The implications on overland height finding are that in order to properly assess target heights over rough terrain a more sophisticated inversion scheme must be utilized. An algorithm that utilizes the knowledge of the propagation physics such as MFP might prove applicable [14].

The general nature of the observed pulse is reproduced well by the pulse synthesis when a modified SEKE propagation model is used with a wide-band synthesis. However, an exact match on a pulse-to-pulse basis is not always achieved due to either: 1) an insufficient propagation model or 2) insufficient characterization of the environment. This latter limitation will be a difficult one to address since the exact nature of the propagated field may require wavelength scale knowledge of the terrain: information not commonly available. It might prove more successful to approach the problem on a statistical basis where the model and the data appear to agree.

References

[1] A. Ishimaru, *Wave Propagation and Scattering in Random Media.* New York: Academic, 1978.
[2] L. Tsang, J. A. Kong, and R. T. Shin, *Theory of Microwave Remote Sensing.* New York: Wiley, 1985.
[3] D. Pairman, S. Belliss, and S. McNeill, "Terrain influences on SAR backscatter around Mt. Taranaki, New Zealand," *IEEE Trans. Geos. Remote Sensing*, vol. 35, pp. 924–932, July 1997.
[4] P. F. Driessen, "Multipath delay characteristics in mountainous terrain—comparison of theoretical predictions with measurement results," in *41st IEEE Veh. Technol. Conf.*, St. Louis, MO, May 1991, pp. 606–609.
[5] J.-P. Rossi, J.-P. Barbot, and A. J. Levy, "Theory and measurement of the angle of arrival and time delay of UHF radiowaves using a ring array," *IEEE Trans. Antennas Propagat.*, vol. 45, pp. 876–884, May 1997.
[6] T. Lo and J. Litva, "Use of a highly deterministic multipath signal model in low-angle tracking," *Proc. Inst. Elect. Eng.*, vol. 138, pp. 163–171, Apr. 1991.
[7] C. C. Lin and Reilly, "Radar terrain clutter model with consideration of propagation effects," in *Proc. 23rd Eur. Microwave Conf.*, Madrid, Spain, Sept. 1993, vol. 1, pp. 478–482.
[8] D. Rana, A. R. Webster and M. Sylvain, "Surface reflection at low-angle propagation," *IEEE Trans. Antennas Propagat.*, vol. 43, pp. 639–52, July 1995.
[9] Y. Liu, S. J. Frasier, and R. E. McIntosh, "Measurement and classification of low-grazing-angle radar sea spikes," *IEEE Trans. Antennas Propagat.*, vol. 46, pp. 27–40, Jan. 1998.
[10] R. M. Narayanan, D. D. Cox, J. M. Ralston, and M. R. Christian, "Millimeter-wave specular and diffuse multipath components of terrain," *IEEE Trans. Antennas Propagat.*, vol. 44, pp. 627–645, May 1996.
[11] F. T. Ulaby, A. Nashashibi, A. El-Rouby, E. S. Li, R. D. De Roo, K. Sarabandi, R. J. Wellman, and H. Bruce Wallace, "95-GHz scattering by terrain at near-grazing incidence," *IEEE Trans. Antennas Propagat.*, vol. 46, pp. 3–13, Jan. 1996.
[12] L. M. Zurk and S. Coutts, "Electromagnetic pulse propagation and scattering from terrain: Experimental observation and comparison with theory," in *IEEE AP-S Int. Symp.*, Montreal, Canada, July 1997, vol. 4, pp. 2576–2579.
[13] L. M. Zurk and B. Geddes, "Experimental observation and modeling of overland height finding," *Proc. IEEE Radar Conf.*, Dallas, TX, May 1998, pp. 411–416.
[14] L. M. Zurk, "Estimation of E-2 overland height finding capabilities," *Proc. Battlesp. Atmosph. Conf.*, San Diego, CA, Dec. 1997, pp. 621–628.
[15] S. Ayasli, "SEKE: A computer model for low-altitude radar propagation over irregular terrain," *IEEE Trans. Antennas Propagat.*, vol. AP-34, pp. 1013–1023, Aug. 1986.

[16] D. E. Kerr, *Propagation of Short Radio Waves.* New York: McGraw-Hill, 1951.
[17] P. Beckman and A. Spizzichino, *The Scattering of Electromagnetic Waves from Rough Surfaces.* New York: Pergamon, 1963.
[18] A. B. Baggeroer, W. A. Kuperman, and P. N. Mikhalevsky, "An overview of matched field methods in ocean acoustics," *IEEE J. Ocean. Eng.*, vol. 18, pp. 401–423, Oct. 1993.
[19] J. K. Jao, "A matched array beamforming technique for low angle radar tracking in multipath," in *IEEE Nat. Radar Conf.*, Atlanta, GA, Mar. 1994, pp. 171–176.
[20] D. R. Gingras, P. Gerstoft, and N. L. Gerr, "Electromagnetic matched-field processing: Basic concepts and tropospheric simulations," *IEEE Trans. Antennas Propagat.*, vol. 45, pp. 1536–1545, Oct. 1997.
[21] M. Papazoglou and J. L. Krolik, "Electromagnetic matched-field processing for target height finding with over-the-horizon radar," in *IEEE Int. Conf. Acoust., Speech, Signal Proc.*, Munich, Germany, Apr. 1997, vol. 1, pp. 559–562.

Lisa M. Zurk received the B.S. in computer science from the University of Massachusetts, Amherst, the M.S. degree in electrical and computer engineering from Northeastern University, Boston, MA, and the Ph.D. degree in electrical engineering from the University of Washington, Seattle, in 1985, 1990, and 1995, respectively.

From 1985 until 1989, she worked as a Software Engineer in research and development for Nova Biomedical, Waltham, MA. From 1990 to 1995 she was a Research Assistant at the Applied Physics Laboratory, Seattle, WA, where she conducted research in the scattering and propagation of electromagnetic waves applied to remote sensing of snow-covered regions and to SAR imaging of the ocean. Since 1996 she has been Technical Staff Member in the Radar Systems Group, MIT Lincoln Laboratory. While at MIT, her research has been in the areas of electromagnetic propagation modeling with application to airborne radar and in underwater acoustic wave propagation with application to sonar signal processing.